HHS Public Access

Author manuscript

J Tissue Eng Regen Med. Author manuscript; available in PMC 2013 March 23.

Published in final edited form as:

J Tissue Eng Regen Med. 2012 October ; 6(9): 673–686. doi:10.1002/term.470.

Aligned Electrospun Scaffolds and Elastogenic Factors for Vascular Cell-Mediated Elastic Matrix Assembly

Chris A. Bashur[1] and **Anand Ramamurthi**[1,2,3,*]

[1]Department of Biomedical Engineering, Cleveland Clinic, Cleveland, OH 44195

[2]Department of Biomedical Engineering, Case Western Reserve University, Cleveland, OH 44106

[3]Department of Bioengineering, Clemson University, Clemson, SC 29634

Abstract

Strategies to enhance the production of organized elastic matrix by smooth muscle cells (SMCs) are critical in engineering functional vascular conduits. Therefore, the goal of this study was to determine the effect of different surfaces (i.e. random and aligned electrospun poly(ε-caprolactone) meshes and two-dimensional controls) and exogenous elastogenic factors on cultured rat aortic SMC phenotype and production of extracellular matrix. This study demonstrated that aligned electrospun fibers guide cell alignment, induce a more elongated cell morphology, and promote a more synthetic phenotype. Importantly, these cells produced greater amounts of elastin-rich matrix per cell on the electrospun scaffolds. In addition, exogenous elastogenic factors severely limited RASMC proliferation and promoted a more synthetic SMC phenotype on electrospun meshes, but they had less effect on two-dimensional controls. Finally, the elastogenic factors induced the SMCs to generate more matrix collagen and elastin on a per cell basis. Together, these results demonstrate the elastogenic benefits of electrospun meshes.

Keywords

Elastin; Vascular Tissue Engineering; Electrospinning; Smooth Muscle Cell; Surface Topography; Growth Factors; Hyaluronan

1. Introduction

Occlusion of peripheral small-diameter (i.e. < 6 mm) arteries cause a decrease in lower-extremity function in 12–20% of seniors (Lloyd-Jones et al., 2009), which can be addressed by bypass grafting with autologous vessels (e.g. saphenous vein). If unavailable due to systemic vascular disease, synthetic vascular prostheses (e.g. Dacron or expanded polytetrafluoroethylene) are used. Synthetic prostheses however tend to incite strong inflammatory responses in the recipient, thrombose, and exhibit compliance mismatches with native vessels (Chlupac et al., 2009). This causes activation of contracting smooth muscle cells (SMCs) and poor luminal endothelialization (Chlupac et al., 2009). Therefore, a

*To whom correspondence should be addressed (ramamua@ccf.org, phone: 216-444-4326, fax: 216-444-9198).

Conflicts of Interest: No conflicts of interest exist

tissue engineered vascular graft that mimics the composition, biology, and mechanics of healthy vessels is needed.

Engineered vascular conduits have thus far been shown to survive up to 4 months of intra-aortal implantation in rats (Campbell et al., 1999; Pektok et al., 2008). However, continuing challenges include compliance mismatches, intimal hyperplasia, and in-graft stenosis, which occur when SMCs switch to an activated phenotype in response to unnatural cues (e.g. biochemical and biomechanical) (Campbell et al., 1999; Pektok et al., 2008). Although structural and mechanical properties of tissue-engineering scaffolds may initially match healthy vascular tissue, as the scaffold degrades, cell-synthesized extracellular matrix (ECM) structures (e.g. collagen and elastic fibers) will determine the load-bearing capacity and elasticity of the construct. Unlike collagen, the production of elastic matrix by vascular cells is hampered by inherently poor tropoelastin synthesis by post-neonatal vascular cells and their limited ability to recruit and crosslink tropoelastin into oriented fibers and higher-order structures (e.g. lamellae) (McMahon et al., 1985; Johnson et al., 1995). This is a significant concern since intact elastic fibers are critical to maintaining vascular homeostasis (e.g. arterial compliance and cell-signaling pathways) (Faury et al., 1998; Li et al., 1998).

Recently, we identified factors (i.e. transforming growth factor beta-1 or TGF-β1, and hyaluronan oligomers or HA-o) that synergistically enhance tropoelastin synthesis and deposition of crosslinked elastic matrix by adult rat vascular SMCs, both healthy and diseased (Joddar and Ramamurthi 2006a; Gacchina and Ramamurthi 2011). While these results are encouraging, further challenges include generating elastic fibers with directional (e.g. circumferential) alignment similar to that within native arteries, which determine the anisotropic mechanics of the aortic wall.

A potential means of influencing SMC phenotype and elastic fiber alignment is with fibrous electrospun meshes. These meshes typically exhibit aligned topographic features 200 nm to 5 μm in size that direct the alignment of ECM-generating cells through contact guidance (denBraber et al., 1996; Yang et al., 2005; Bashur et al., 2006), and consequentially align the ECM produced by the cells in the same direction (Wang et al., 2003). In addition, meshes can provide a porous three-dimensional (3-D) microenvironment conducive to cell infiltration and matrix deposition (Vaz et al., 2005). Previous research has shown that the topographic features of electrospun meshes influence the attachment, spreading, alignment, and phenotype of several cell types (e.g. rat bone marrow stromal cells (BMSCs) and rat embryonic hippocampal neurons (Bashur et al., 2009; Lee et al., 2009a; Lee et al., 2009b)). While SMCs have also been shown to align with aligned electrospun fibers (Zhang et al., 2008; Dong et al., 2010), their poor ability to synthesize tropoelastin and deposit elastic fibers still needs to be addressed. Therefore, understanding the combined impact of substrate-derived cues and elastogenic factors on SMCs phenotype and ECM synthesis is important in engineering a vascular construct.

In this study, we specifically investigated the impact of electrospun meshes, alignment of electrospun fibers, and the addition of exogenous elastogenic factors on enhancement and guidance of elastic fiber formation. Electrospun meshes, consisting of random and aligned poly(ε-caprolactone) (PCL) fibers were prepared. Rat aortic smooth muscle cells (RASMCs)

were cultured on electrospun meshes, smooth PCL films, and tissue culture polystyrene (TCPS) wells, both with and without exogenous factors, to determine their effects on cell density, morphology, alignment, messenger ribonucleic acid (mRNA) expression, and possible enhancement in cellular deposition of a directionally-oriented elastic matrix.

2. Materials and Methods

2.1 Materials

All disposables, chemicals, and biological supplies were purchased from VWR (West Chester, PA) unless specified otherwise. Antibodies were purchased from Abcam (Cambridge, MA), unless specified otherwise. PCL (inherent viscosity 1.0 – 1.3 dL/g in chloroform) was purchased from Lactel Absorbable Polymers (Pelham, AL). TGF-β1 was purchased from Peprotech (Rocky Hill, NJ). The HA-o mixture contained 75% w/w HA 4mers (MW: 756 Da) and was produced in the lab by enzymatic digestion of high molecular weight HA (Genzyme Biosurgery, Cambridge, MA) with testicular hyaluronidase (Sigma Aldrich, Saint Louis, MO; 37°C, 16 h, 160 U/mg), as described previously (Joddar and Ramamurthi 2006b).

2.2 Electrospinning and Spin-coating

PCL was electrospun from a 90% v/v chloroform and 10% dimethylformamide (DMF) solution to form meshes with controlled average fiber diameters and degrees of orientation. Specific electrospinning parameters included a 16 – 18% w/v PCL solution, a 22 gauge needle, 11 kV voltage gradient, 3 mL/h flow rate, and 15 cm throw. An adjustment in the solution concentrations (i.e. 18% to 17% and 18% to 16% w/v for random and aligned meshes, respectively) for studies with the addition of factors was necessary to maintain a similar average fiber diameter, since a different batch of PCL (i.e. 1.15dL/g to 1.21dL/g) was used. Fiber alignment was induced using a grounded, aluminum foil-wrapped drum (12.7 cm diameter) with the target rotating at 1 600 rpm to mechanically induce fiber orientation, similar to previous studies (Bashur et al., 2006). The drum was rotated at 30 rpm to create meshes containing randomly-oriented fibers. The target was moved laterally to ensure uniformity of mesh thickness along the length of the drum. By setting the electrospinning time as 1 h, we were able to produce meshes with an average thickness of 63 ± 5.0 μm (n = 8 sections). After electrospinning, the meshes were allowed to air-dry, peeled off the aluminum foil, and then cut into strips. Spin-coated PCL films were prepared from 4% w/v solutions of PCL in dichloromethane. Briefly, a volume of 350 μL was added to 18 mm diameter glass coverslips, and spun at 5 000 rpm for 15 s (WS-650Mz NPP Single Wafer Spin Processor, Laurell Technologies Corporation, North Wales, PA). The samples were stored in a desiccator until use. For fluorescent visualization of the PCL fibers, electrospun meshes were incubated for 1 h in an aqueous 4μL/mL solution of the hydrophobic 1,1′-dilinoleyl-3,3,3′,3′-tetramethylindocarbocyanine perchlorate (DiI) stain (Invitrogen, Carlsbad, CA).

For cell culture, electrospun meshes were placed between poly(dimethylsiloxane) rings (Sylgard® 184, Dow Corning Corporation, Midland, MI) with an inner area of 1.7 cm^2, and pinned with stainless steel minutin pins (Fine Science Tools, Foster City, CA). The mesh

constructs and spin-coated films (area = 2.5 cm^2) were placed in 12 well plates (area = 3.1 cm^2) and sterilized with ethylene oxide.

2.3 Scaffold Characterization

2.3.1 Scanning Electron Microscopy (SEM)—Fiber diameter, degree of fiber orientation, and mesh thickness were determined from SEM images. For SEM, the electrospun meshes were mounted onto aluminum stubs and imaged without sputtercoating using a Hitachi TM-1000 Tabletop microscope (Gaithersburg, MD) operating at 15kV with a working distance of 6 mm. Spin-coated surfaces were imaged using a Hitachi S4800 (Gaithersburg, MD) at 1 kV and a working distance of 6 mm. Mesh thicknesses were measured on samples frozen in liquid nitrogen and then cut transversely. The resultant images were imported into Image J (National Institutes of Health, Bethesda, MD) for analysis (≥3 images/condition). The degree of orientation was characterized by angular standard deviation (ASD), where a lower angular standard deviation indicates a mesh containing more aligned fibers (Bashur et al., 2006).

2.4 Cell Isolation and Culture

2.4.1 Impact of Topography and Mesh Alignment on ECM Synthesis—Healthy RASMCs were isolated from 200-250 g male Sprague-Dawley rats (Harlan, Dublin, VA), in accordance with the Institutional Animal Care and Use Committee (IACUC) procedures at the Medical University of South Carolina (i.e. the performing site at the time of this study). Primary RASMCs were obtained from adult rat aortal explants, and expanded in culture with Dulbecco's Modified Eagle Medium (DMEM)/F12 containing 20% v/v fetal bovine serum (FBS; PAA Laboratories Inc, Dartmouth, MA) and 1% v/v penicillin-streptomycin (Fisher Scientific, Pittsburgh, PA). Prior to cell culture, the substrates were equilibrated with sterile 50% v/v ethanol, rehydrated with DMEM/F12 medium, and then soaked for 3 h in DMEM/F12 containing 20% v/v FBS and 1% v/v penicillin-streptomycin. Passage 3 cells were seeded on electrospun PCL meshes and spin-coated PCL films (controls). The meshes were seeded The meshes were seeded with 3–8×10^3 cells/cm^2 (3×10^3 and 8×10^3 cells/cm2 for replicates 1 and 2, respectively) and cultured in medium containing 10% v/v FBS. After 2, 6, and 21 days of culture, the cell layers were analyzed for cell density, morphology, orientation, phenotype, and for cellular matrix generation.

2.4.2 Impact of Exogenous Factors on Elastic Matrix Deposition—Studies were performed as described in section 2.4.1, except for protocol changes necessary to further improve cell attachment, proliferation, and the production of elastic matrix. RASMCs seeded on tissue culture polysytrene wells served as controls. In additon, surfaces were soaked for 3 h in a 1 μg/mL solution of human plasma fibronectin (Calbiochem, New Zealand) prior to culture, instead of culture medium, to improve cell attachment. The cells were seeded at 1.5 × 10^4 cells/cm^2, and two days afterward, cultured in medium supplemented with TGF-β1 (i.e. 1 ng/mL) and HA-o (i.e. 0.2 μg/mL) shown previously to have elastogenic effects (Kothapalli et al., 2009). After 2, 6, and 21 days of culture, cell layers were harvested and analyzed for cell density, morphology, orientation, phenotype, and/or for accumulation of ECM.

2.5 Biochemical Assays

2.5.1 Cell Density—A deoxyribonucleic acid (DNA) assay was performed at 2, 6, and 21 days post-seeding to determine cell density and to ascertain cell proliferation. DNA content was quantified using a fluorometric assay described by Labarca and Paigen (Labarca and Paigen 1980). Briefly, cell layers were scraped off the wells and films, suspended in 1 mL of NaCl/Pi buffer (4 M sodium chloride, 50 mM sodium bicarbonate, 2 mM EDTA, and 0.02% w/v sodium azide; pH 7.4), and sonicated 1 min to lyse cells and release DNA. An aliquot was removed for biochemical analysis of protein content, with the remaining volume retained for DNA quantification with Hoechst 33258 dye. Cell densities were calculated based on the estimate of 6 pg of DNA/cell.

2.5.2 Elastin Content—A Fastin® assay (Accurate Chemical and Scientific Corporation, Westbury, NY) was used to quantify the total amount of matrix-elastin (i.e. the alkali-soluble and alkali-insoluble fractions combined), as described previously (Joddar and Ramamurthi 2006a). The more highly crosslinked alkali-insoluble fraction was measured separately, and served as a measure of the degree of crosslinking in the matrix elastin. Briefly, the protein samples (see Section 2.5.1) were treated with 0.1 M sodium hydroxide (98°C, 1 h) and centrifuged at 3000 rpm for 10 min. The supernatant was assayed for alkali-soluble matrix elastin using the Fastin® assay, and for collagen via a hydroxyl-proline (OH-Pro) assay (see Section 2.5.3). The pellet of alkali-insoluble matrix elastin was solubilized with 0.25 M oxalic acid (98°C, 1 h), concentrated with a low molecular weight cut-off filter (10 000 Da), and then assayed with the Fastin® assay. The Fastin® assay was performed as described in the manufacturer's protocol. The measured elastin protein amounts were normalized to the corresponding cell number, as determined by the amount of DNA.

2.5.3 Collagen Content—An OH-Pro assay was used to estimate the amounts of collagen deposited by cells seeded on electrospun constructs and on control surfaces, as described previously (Stegemann and Stalder 1967; Joddar and Ramamurthi 2006a). The alkali-soluble fraction described in Section 2.5.2, containing solubilized matrix collagen, was hydrolyzed at 110°C for 16 h and then dried at 110°C. Aliquots (20 μL) of the reconstituted residues were assayed with the OH-Pro assay. Collagen amounts were then calculated on the basis of 13.2% w/w OH-Pro content of collagen, and normalized to DNA content of the corresponding source cells.

2.6 Imaging and Quantitative Analysis

2.6.1 Live/Dead Assay—Cell viability was determined using a fluorescence-based live/dead assay (Invitrogen, Carlsbad, CA) at 6 days of culture. The live cells were stained with calcein-AM (green) and dead cells with compromised membranes stained with ethidium homodimer (red).

2.6.2 Immunofluorescent Detection of Phenotypic Markers and ECM Proteins —Immunofluorescence was used to determine RASMC morphology, alignment, phenotype, and the cellular generation of matrix proteins at 21 days of culture, similar to previous studies (Kothapalli et al., 2009). Briefly, the cells on electrospun meshes were fixed with 4% w/v paraformaldehyde for 20 min, the meshes were cut into 4 pieces, the cells were

permeabilized with 0.1% v/v Triton X-100 (VWR) for 10 min, and the cells were blocked with 5% v/v goat serum (PAA Laboratories Inc.). Cell phenotype was assessed with primary antibodies that detected SMC markers of both contractility (Hoenig et al., 2005) (i.e. transgelin or SM22α, calponin, caldesmon, and α-smooth muscle actin) and activation (Majack et al., 1988) (i.e. thrombospondin 1 and osteopontin) (Abcam, Cambridge, MA), and visualized with secondary antibodies conjugated to Alexa 488, 568, or 594 probes (Invitrogen). The presence of matrix proteins was detected with primary antibodies (i.e. rabbit anti-rat and mouse anti-rat) against collagen type 1 and elastin (Abcam). Cell nuclei were visualized with the nuclear stain 4′,6-diamino-2–phenylindole dihydrochloride (DAPI) contained in the mounting medium (Vectashield, Vector Labs, CA). Electrospun fibers were visualized with DiI stain. Imaging was performed on an Olympus IX51 fluorescent microscope (Pittsburgh, PA) and with a Leica scanning confocal microscope (Heidelberg, Germany). For confocal images, z-stack maximum projections were created from images acquired at 1 μm intervals across the thickness of the sample, using Leica LAS AF software. The brightness and contrast were adjusted equally for all cases and for the immunofluorescent labeling control (i.e. no primary antibody). Cell morphology and alignment were measured from these images using ImagePro Plus software. Cell aspect ratio, cell area, and the degree of cell alignment of recognizable cells were calculated using a custom macro designed to adjust image fluorescence intensity and pixel deviation, count cells (e.g. nuclei or cytoskeletal outline), remove cells on the edge of the image, auto-split objects, allow for further manual adjustment, and export morphological results.

2.7 Real time-Polymerase Chain Reaction (PCR)

Expression of SMC markers and matrix proteins were determined quantitatively with real time (RT)-PCR (Bashur et al., 2009). Briefly, total RNA was isolated from the cells on days 6 and 21 using the RNeasy Mini Kit (Qiagen, Valencia, CA) according to manufacturer's instructions. The amount of RNA in the lysates and the RNA integrity number (RIN) were quantified with an Agilent 2100 Bioanalyzer (Santa Clara, CA). Equal masses of RNA (100 ng for day 6 samples) were reverse transcribed using iScript® cDNA synthesis kit (Bio-Rad Laboratories, Hercules, CA) according to the manufacturer's instructions. More mRNA (i.e. 300 ng) was reverse transcribed for day 21 samples due to greater availability. RT-PCR was performed in the ABI 7500 Real-Time PCR System (Applied Biosystems, Foster, CA) using 5 ng complementary DNA (cDNA) for day 6 samples and 15 ng cDNA for day 21, with Power SYBR®Green Master Mix (Applied Biosystems). Specific primers were used for β-actin (*Actb*; the internal reference), collagen 1α1 (*Col1a1*), elastin (*Eln*), osteopontin (*Osp*), thrombospondin 2 (*Thbs2*), α-smooth muscle actin (*Acta2*), caldesmon (*Cald1*), and smooth muscle myosin heavy chain (*Myh11*). The *Col1a1* (Bashur et al., 2009), *Actb* (Bashur et al., 2009), and *Eln* (Kothapalli et al., 2009) primers were designed in previous studies. Other primer sequences were designed in PerlPrimer (Marshall 2004) using the Ensembl and NCBI databases (Table 1) and purchased from Applied Biosystems (Carlsbad, CA). Quantification of gene expression was reported as $2^{-\Delta\Delta Ct}$ using the comparative threshold method (ΔΔCt) (Livak and Schmittgen 2001). Amplification without cDNA and amplification of isolated RNA were performed as controls to verify the integrity of the amplification process. The *Actb* internal reference gene Ct values were similar for all samples, with 18.8 ± 0.95 Ct for day 6 samples and 16.9 ± 1.4 Ct for day 21 samples.

2.8. Statistics

Cell culture with and without exogenous factors were performed in separate studies. Results are presented as the mean ± standard deviation for $n = 4$ samples/substrate for SEM analysis of electrospun meshes. A total of $n = 12$ samples/substrate were assayed to determine the effect of different surfaces on cell density and generated matrix, and $n = 6$ cultures/condition were assayed in exogenous factors studies. Nuclear morphology was determined with $n = 4$ cultures/condition (>27 cells/culture and >100 cells/sample for 6 and 21 days of culture, respectively). Overall cell morphology was determined with $n \geq 49$ cells/condition. Gene expression was determined for $n = 6$ cultures/condition. All studies were replicated (i.e. performed twice) using separate batches of electrospun meshes and RASMCs to ensure reproducibility. Statistical analysis was performed with SPSS software and statistical significance determined using one-way analysis of variance (ANOVA) with post-hoc comparisons using the Fisher Least Significant Difference method for a significance criterion of $p \leq 0.05$.

3. Results

3.1. Electrospun Mesh Characterization

Highly aligned and random electrospun meshes with micrometer and sub-micrometer diameter fibers were fabricated (Figure 1). The average fiber diameters and degree of orientation (i.e. 1.0 ± 0.34 and 1.1 ± 0.28 μm, 25 ± 2.8 and 56 ± 3.8°; n = 4 for aligned and random meshes, respectively) were comparable for all studies and replicates. Some variation in fiber diameter was however present between studies, with average fiber diameters for the aligned and random meshes ranging from 0.70 to 1.3 μm and 0.73 to 1.3 μm, respectively (≥ 3 images and > 100 fibers/study or replicate). The average thickness of the electrospun meshes was 63 ± 5.0 μm.

3.2. Impact of Substrate on Cell Morphology and Behavior

RASMCs were cultured on aligned meshes, random meshes, and spin-coated PCL surfaces that were pre-adsorbed with serum proteins to aid cell attachment. At day 6, most of the cells were viable and well spread on the substrates (Figure 1). The cells infiltrated throughout the thickness of the aligned and random meshes, although more cells appeared to be localized close to the surface layers (Figure 2). RASMCs seeded on the meshes (i.e. aligned and random) exhibited decreased nuclear area ($p \leq 0.009$ vs. 2-D spin-coated surfaces), as quantified from DAPI stained nuclei (Figure 3). Corresponding increases in the nuclear aspect ratio were also measured in cells cultured on aligned meshes ($p \leq 0.040$ vs. random meshes and spin-coated films). The morphology of cell nuclei was transient and varied between 6 and 21 days of culture. With nuclear area in particular, the value increased over time for cells cultured on spin-coated films ($p \leq 0.001$ vs. 6 days) but decreased for cells cultured on random meshes ($p = 0.045$ vs. 6 days), indicating that 2-D and 3-D surfaces promote different cellular responses. Similar trends were observed in cytoskeletal morphology, although differences between conditions were more significant than that observed with nuclear morphology. The decreases in nuclear and cytoskeletal area for cells within the aligned compared to the spin-coated condition were 15 and 65%, respectively; while the increase in aspect ratios were 20 and 120% for nuclei and cells, respectively. The

cytoskeletal angular deviations (i.e. degrees of alignment) were 15, 40, and 72° for aligned mesh, random mesh, and spin-coated, respectively.

The RASMCs increased in density over 21 days in culture on all substrates, indicative of cell proliferation (Figure 3). At 6 and 21 days of culture, adhered cell densities were significantly higher on electrospun meshes ($p \leq 0.025$ vs. spin-coated films). Overall, collagen matrix synthesis was greater on spin-coated PCL films (96 ± 35 μg) than on aligned (72 ± 44) and random (74 ± 42) meshes. On a per cell basis, collagen synthesis was at least 5 times higher on the spin-coated surfaces ($p \leq 0.001$ vs. random and aligned meshes) (Figure 3). The total amounts of matrix elastin deposited on aligned and random meshes were 48 ± 29 and 43 ± 22 μg, respectively; which represented a greater than 7.5 fold increase over spin-coated PCL films (i.e. 5.7 ± 6.6 μg). Elastic matrix synthesis (i.e. both alkali-soluble and alkali-insoluble fractions) was still significantly greater, on a per cell basis, on the electrospun mesh ($p \leq 0.036$ vs. spin-coated film) (Figure 3). Immunofluorescent imaging of 21 day cell cultures, show intracellularly-localized collagen type 1, likely procollagen, a few sporadic clumps of extracellular elastin, and limited if any complete collagen or elastic fibers (Figure 4). These images also show that cells presented markers of both contractility (i.e. SM22α) and activation (i.e. thrombospondin 1) (Figure 4). Additionally, levels of thrombospondin appeared to be lower for cells cultured on spin-coated films than those cultured on the electrospun meshes.

3.3. ECM Synthesis in the Presence of Growth Factors

As in the first study, RASMCs attached readily onto electrospun meshes, random and aligned, and on TCPS (i.e. 2-D controls). RASMCs cultured on the electrospun meshes, without exogenous factors, actively proliferated and exhibited higher cell densities at 21 days ($p \leq 0.001$vs. TCPS) (Figure 5). Cultures maintained in the presence of exogenous factors exhibited lower cell density at 21 days regardless of the substrate ($p \leq 0.003$ vs. no-factor controls). Nuclear areas and aspect ratios did not vary between cultures maintained in the presence or absence of the factors, for any of the substrates (Figure 6). As noted in section 3.2 for RASMCs cultured on aligned meshes, the nuclear area was lower ($p \leq 0.001$ vs. TCPS) but the nuclear aspect ratio higher ($p \leq 0.004$ vs. TCPS) compared to RASMCs cultured on 2-D surfaces. In addition, RASMCs exhibited a lower angular deviation (i.e. higher degree of alignment) when cultured on aligned meshes compared to culture on TCPS wells.

On a per cell basis, synthesis of matrix collagen and alkali-soluble matrix elastin were increased in the presence of HA-o and TGF-β1, independent of substrate ($p \leq 0.017$ and 0.014 vs. no-factor controls, respectively). Synthesis of alkali-insoluble matrix elastin was also increased in the presence of the factors ($p = 0.038$ and 0.047 vs. no-factor controls for aligned mesh and TCPS, respectively) (Figure 5). When cultured with elastogenic factors, RASMCs on the electrospun meshes synthesized less matrix collagen ($p \leq 0.001$vs. TCPS); however, there were no significant differences in elastic matrix synthesis. The respective amounts of matrix collagen deposited on aligned meshes, random meshes, and TCPS wells were similar both in the presence of factors (31 ± 30, 82 ± 29, and 96 ± 49 vs. no-factor controls, respectively) and in their absence (56 ± 21, 91 ± 38, and 99 ± 42 vs. no-factor

controls, respectively). However, total elastic matrix deposition on aligned meshes, random meshes, and TCPS wells was lower in the presence of factors (240 ± 130, 230 ± 110, and 130 ± 66 μg vs. no-factor controls, respectively) than in their absence (690 ± 180, 590 ± 220, and 340 ± 88 vs. no-factor controls, respectively). Immunofluorescent images show that, like the first study, the RASMCs present both contractile and activated markers (Figure 7), with thrombospondin and α-smooth muscle actin (α-SMA) levels appearing to be lower and SM22α levels appearing to be higher in the presence of the factors, both on the aligned and random meshes.

The mRNA expression of the RASMCs demonstrated transience between 6 and 21 days of culture, regardless of the substrate. At 6 days post-seeding, significant differences in gene expression were observed for RASMCs cultured on electrospun meshes ($p \leq 0.001$, 0.043, 0.001, 0.001, and 0.034 vs. TCPS for *Eln, Osp, Myh11, Acta2, and Cald1*, respectively) (Figure 8). Differences in expression of genes were also observed between cells cultured in the presence of HA-o and TGF-β1 factors, and those in their absence. These differences were primarily observed when cells were cultured on electrospun meshes ($p \leq 0.003$, 0.031, and 0.002 for *Col1a1, Osp, and Thbs2*, respectively). There was no significant change in expression of tropoelastin and markers of contractility by RASMCs cultured on electrospun meshes in the presence of elastogenic factors, although *Myh11* mRNA expression decreased ($p \leq 0.006$ for aligned only). Interestingly, no difference in mRNA expression were observed with the addition of factors on TCPS surfaces, with the exception of *Myh11* ($p \leq 0.001$ for aligned only). At day 21 post-seeding, *Thbs2* expression by RASMCs on the aligned mesh was significantly lower with the addition of exogenous factors ($p \leq 0.016$), but no other conditions were statistical significant (Figure 8). The *Myh11*expression appeared to decrease on the electrospun meshes with the addition of factors, but was not statistically significant.

4. Discussion

The poor elastogenicity of post-neonatal vascular cells is one of the most significant challenges to creating functional, tissue-engineered vascular replacements (Patel et al., 2006). Several factors have been shown to effect tropoelastin production and elastic matrix assembly. The matrix glycosaminoglycan (GAG) hyaluronan (HA) and proteoglycans (e.g. versican) have been shown to influence elastic matrix deposition, fiber organization, and stabilization (Bressan et al., 1986; Fornieri et al., 1987; Olin et al., 2001; Isogai et al., 2002; Cantor and Turino 2004). In addition, overexpression of endogenous TGF-β1 has been shown to decrease proteolysis of elastin and collagen in rat abdominal aortic aneurysms, increase generation of an ECM layer rich in collagen and elastic fibers, and enhance lysyl oxidase (LOX) production by vascular cells *in situ* (Losy et al., 2003; Dai et al., 2005). The combination of these factors (i.e. HA-o and TGF-β1) has previously been shown to synergistically induce adult rat SMCs in 2-D cultures and enhance tropoelastin synthesis, recruitment, and crosslinking into elastic fibers (Joddar and Ramamurthi 2006a; Kothapalli et al., 2009). However, the alignment of elastic matrix structures is also vital since anisotropic mechanical properties are required for vascular tissues. Incorporating electrospun meshes with aligned fibers and high porosity may address this challenge since electrospun meshes are able to direct SMC alignment (Yang et al., 2005; Zhang et al., 2008;

Dong et al., 2010) and influence collagen fiber alignment (Wang et al., 2003). Therefore, the goals of this study include (a) producing scaffolds to direct the alignment of elastic matrix and (b) determining how SMC response differs between culture on these scaffolds and on 2-D surfaces, in combination with elastogenic factors.

PCL was specifically selected as the scaffold material because the tensile strength of electrospun PCL meshes (i.e. 1.2 MPa) is similar to human coronary arteries (i.e. approximately 1.8 MPa) (Holzapfel et al., 2005; Vaz et al., 2005), and because single PCL fibers exhibit yield strain (i.e. 20 ± 10%) higher than typical strains exhibited by small human arteries (i.e. human femoral arteries expand in diameter by only 2–15% during the cardiac cycle) (Dobrin 1978; Tan et al., 2005). These human vessels are the ultimate application for the tissue engineering strategies described in this study. A second motivation for selecting PCL is that it degrades over a time frame (1–3 years) that should allow generation of sufficient structural matrix for the construct to withstand physiologic loads and forces (Nair and Laurencin 2007).

In this study, PCL fibers were electrospun with diameters of approximately 1 μm. These electrospun meshes exhibited effective pore diameters large enough to permit cell infiltration throughout the thickness of the mesh, which agrees with previous studies (Vaz et al., 2005). In addition, these PCL meshes supported greater cell densities than the 2-D surfaces (i.e. PCL films and TCPS wells), potentially due to the greater surface area for enhanced cell attachment and proliferation (Bashur et al., 2009). Thus, differences were observed between substrates with the same chemistry but different physical structures. Specifically, the electrospun meshes exhibited more topographic features but also represented structures that could potentially be more readily deformed by the cells. Published studies have investigated a variety of cell types including SMCs from various sources, topographic irregularities at various scales of measurement, and material compliances, which may explain why SMC proliferation has been shown to both increase and decrease on electrospun meshes compared to 2-D control surfaces (Stankus et al., 2006; Dong et al., 2010). These results strongly suggest that variations in the complex interaction between components of the cell microenvironment can affect cell behavior.

One of the primary goals of this study was to determine the effect of different surface topographies (i.e. aligned PCL mesh, random PCL mesh, and spin-coated PCL films) on RASMC phenotype and matrix synthesis. Throughout 21 days of culture, the RASMCs that adhered on the aligned meshes were found to align along the fibers and to exhibit a more elongated morphology than RASMCs cultured on 2-D surfaces, suggesting that a greater percentage of the cells exhibit a spindle-shaped SMC morphology. This elongation was observed in both the nuclei and the cytoskeleton, and confirms prior observations that cell nuclei can be used as an alternative quantitative measure of morphology and alignment (Richard et al., 2007). This is particularly advantageous in analyzing confluent cell layers wherein edges of individual cells are difficult to determine. However, nuclear shape appears to be a less sensitive predictor of morphological differences between cells, since differences in nuclear areas between cells cultured on aligned meshes and spin-coated films were lower relative to the differences in cytoskeletal areas of the same cells (i.e. < 4 times). Although RASMCs cultured on aligned fibers were also more aligned and less elongated relative to

those cultured on random meshes, the differences in cell morphology were more significant between RASMCs cultured on 2-D substrates and 3-D meshes (i.e. both random and aligned). The RASMCs cultured on both spin-coated films and TCPS wells were significantly more spread than on the meshes. Similar results have previously been observed with endothelial, mesenchymal and fibroblastic cells types (Bashur et al., 2006; Bashur et al., 2009). These results may be related to differences in topographical features and separately, compliance of substrates (Yeung et al., 2005).

The outcomes of the study of cell proliferation and morphology support the understanding that cell behavior is impacted by both mechanical cues and by topographic features and suggests that additional differences in cell phenotype can be expected. SMCs are frequently described as exhibiting either contractile or synthetic phenotypes, though in actuality, a continuum exists between these two extreme phenotypic states (Hu et al., 2008; Beamish et al., 2010). When *in vivo*, contractile SMCs exhibit a more pronounced contractile cytoskeleton with limited proliferation and ECM production. The opposite characteristics are typically observed with more synthetic SMCs; however, several groups have demonstrated that *in vitro* cell cultures present unique microenvironments. SMCs partially lose their contractile characteristics when cultured on most surfaces (Worth et al., 2001; Zhang et al., 2008; Dong et al., 2010), and, more importantly, this response has been shown to vary between 2-D and 3-D surfaces (Peyton et al., 2008). Several groups have demonstrated an inverse relationship between SMC proliferation and collagenous ECM synthesis on 2-D surfaces and 3-D gels (i.e. collagen) (Li et al., 2003; Stegemann and Nerem 2003). In this study, we have also observed this inverse relationship between RASMC proliferation and collagen synthesis both on smooth PCL films/TCPS wells and 3-D electrospun PCL meshes. In addition, collagenous and elastic matrix generation showed opposite trends, which is similar to that shown previously (Davidson et al., 1997; Hu et al., 2008). On the meshes, cellular synthesis of elastin was enhanced relative to PCL films/ TCPS wells. This may be due to decreased stiffness of the substrate (i.e. greater ability for cell traction forces to deform the substrate), a mechanism that has been proposed previously (Gao et al., 2008).

Differences in cell responses on 2-D and 3-D surfaces were also evident in the mRNA expression profiles (i.e. ECM proteins and SMC markers) and in the matrix produced by the RASMC. This demonstrates the correlation between cell morphology and cellular function (Richard et al., 2007). Early in culture (i.e. after 6 days) the cells on the meshes exhibited a significant decrease in expression of contractile SMC markers (e.g. *Myh11*, *Acta2*, and *Cald1*) and an increase in expression of activated SMC markers (e.g. *Osp* and *Thbs2*) compared to those on 2-D TCPS surfaces, which agrees with the enhanced proliferative response of the RASMCs on electrospun meshes. The SMCs exhibited transience in mRNA expression that has been observed previously and is expected because of their phenotypic plasticity (Hu et al., 2008; Zhang et al., 2008). By day 21 of culture, RASMCs were not as sensitive to the different surfaces, although *Thbs2* expression was still significantly higher on electrospun meshes. Despite observations that elastic matrix on the electrospun meshes was greater than on the TCPS substrates, no corresponding differences were noted in the ECM mRNA expression. This suggests that post-transcriptional mechanisms of tropoelatin

recruitment and crosslinking by lysyl oxidase (LOX), and not elastin transcription itself, are affected by the substrate (Kothapalli and Ramamurthi 2009).

A second goal of this study was to determine the effect of elastogenic factors (i.e. HA-o and TGF-β1) on RASMC response and elastic matrix synthesis. In the presence of the factors, regardless of substrate, cell number at 21 days was several fold lower than corresponding factor-free control cultures, suggesting suppressed cell proliferation. These results agree with our prior observations (Kothapalli et al., 2009). This effect is most likely due to the TGF-β1, which has been shown to be both a positive and negative regulator of cell proliferation, depending on the cell type, exposure dose, and the culture conditions (Majack et al., 1990; Sajid et al., 2000). While this study did not explore the detailed mechanism, the result is confirmed by decreased thrombospondin mRNA and protein levels when RASMCs were cultured with elastogenic factors. One of the proposed mechanisms of interaction between thrombospondin and TGF-β1 is that thrombospondin binds to $\alpha_v\beta_3$ integrin and leads to extracellular signal-regulated kinase (ERK) signaling (Sajid et al., 2000). A body of evidence has shown however that the presence of thrombospondin is necessary for SMC proliferation (Sajid et al., 2000).

In addition to suppressing cell proliferation, the HA-o and TGF-β1-induced RASMCs on both 2-D substrates and 3-D meshes to synthesize significantly more ECM (i.e. increase in matrix collagen and elastin per cell). Factor-induced increases in *Col1a1* and *Osp* mRNA expression and corresponding decrease in *Myh11* mRNA expression by RASMCs early in culture (i.e. at 6 days post-seeding) corroborate this phenotypic switch at a transcriptional level. It is also worth noting that the nuclear areas and mRNA expression of cytoskeletal markers, with the exception of *Myh11*, were not significantly decreased by the exogenous factors. Since *Myh11* is one of the contractile markers that SMCs lose the earliest when they become more synthetic (Worth et al., 2001), this result suggests that the factor-induced decrease in contractile marker expression is less significant compared to the corresponding increase in expression of synthetic markers. In addition, although factors increased RASMC osteopontin mRNA expression, the overall level of the marker protein, as observed in immunofluorescent images, was very low. No mineralization of the ECM was noted previously when these factors were provided (Kothapalli et al., 2009). Notably, factor-induced increases in the synthesis of both elastic and collagenous matrix by RASMCs do not correspond to similar fold-increases in elastin and collagen mRNA expression. This result suggests that the elastogenic factors may be influencing transcription of genes for ECM crosslinking (e.g. LOX), which we did not study, or may be post-transcriptionally facilitating matrix precursor recruitment and crosslinking with LOX (Kothapalli and Ramamurthi 2009).

Importantly, the elastogenic factors did not appear to have the same effect on RASMCs cultured on electrospun meshes compared to those cultured on 2-D surfaces. No differences in gene expression, other than *Myh11*, were observed when RASMCs were cultured on TCPS surfaces with and without elastogenic factors. However, total matrix production increased with elastogenic factors independent of the type of surface. Overall, these differences can be explained on the basis of the diversity of effects TGF-β1 is known to have on SMCs, which involve different signaling cascades (Pardali et al., 2010).

Although several beneficial effects of electrospun meshes have been demonstrated, the total amounts of cell synthesized elastic matrix need to be further increased and this matrix should be more highly crosslinked. One possible way to improve matrix yield, would be to deliver the elastogenic factors, or TGF-β1 in particular, only after the cells have reached a sufficient density. Adjusting the doses of elastogenic factors may also increase tropo- and matrix elastin production of RASMCs, as this has previously been shown to be effected by the density and ratio of the factors (Joddar and Ramamurthi 2006b; Kothapalli et al., 2009). In addition, exogenous LOX may increase both the amount of crosslinked elastic matrix and the organization and maturation of that matrix (Kothapalli and Ramamurthi 2009). Finally, the elastic matrix yield can be increased with the use of a different cell source, since less differentiated neo-natal and progenitor cells in particular are inherently more elastogenic (Fornieri et al., 1992).

5. Conclusions

This study demonstrated that electrospun fibers guide RASMC alignment. In addition, the RASMCs on the aligned meshes exhibited a significantly more elongated morphology and exhibited a more synthetic phenotype than on 2-D surfaces (i.e. spin-coated PCL films and TCPS wells). Importantly, these cells produced more elastin-rich matrix per cell on the electrospun scaffolds than on spin-coated films (i.e. less collagen but more matrix elastin). The exogenous elastogenic factors severely limited RASMC proliferation over 21 days and promoted a switch to a more synthetic SMC phenotype when cultured on electrospun meshes. However, these effects of exogenous factors were not generally observed with RASMCs cultured on 2-D TCPS wells. Finally, the cells produced more matrix collagen and elastin per cell with the addition of the elastogenic factors, even though the total matrix amount was limited by the suppressed cell proliferation. Together, these results demonstrate the benefits of electrospun meshes in producing a small-diameter vascular graft.

Acknowledgments

This study was supported by NIH Grants:

National Heart, Lung, and Blood Institute (5R01HL 092051-02)

National Institute of Biomedical Imaging and Bioengineering (EB006078-01A1).

This study was supported by NIH Grants through the National Heart, Lung, and Blood Institute (HL092051-01A1 and HL092051-01S) and the National Institute of Biomedical Imaging and Bioengineering (EB006078-01A1) awarded to Ramamurthi A.

References

Bashur CA, Dahlgren LA, Goldstein AS. Effect of fiber diameter and orientation on fibroblast morphology and proliferation on electrospun poly(D, L-lactic-co-glycolic acid) meshes. Biomaterials. 2006; 27:5681–5688. [PubMed: 16914196]

Bashur CA, Shaffer RD, Dahlgren LA, Guelcher SA, Goldstein AS. Effect of fiber diameter and alignment of electrospun polyurethane meshes on mesenchymal progenitor cells. Tissue Eng Part A. 2009; 15:2435–2445. [PubMed: 19292650]

Beamish JA, He P, Kottke-Marchant K, Marchant RE. Molecular regulation of contractile smooth muscle cell phenotype: implications for vascular tissue engineering. Tissue Eng Part B Rev. 2010; 16:467–491. [PubMed: 20334504]

Bressan GM, Pasquali-Ronchetti I, Fornieri C, Mattioli F, Castellani I, Volpin D. Relevance of aggregation properties of tropoelastin to the assembly and structure of elastic fibers. J Ultrastruct Mol Struct Res. 1986; 94:209–216. [PubMed: 3805787]

Campbell JH, Efendy JL, Campbell GR. Novel vascular graft grown within recipient's own peritoneal cavity. Circ Res. 1999; 85:1173–1178. [PubMed: 10590244]

Cantor JO, Turino GM. Can exogenously administered hyaluronan improve respiratory function in patients with pulmonary emphysema? Chest. 2004; 125:288–292. [PubMed: 14718453]

Chlupac J, Filova E, Bacakova L. Blood vessel replacement: 50 years of development and tissue engineering paradigms in vascular surgery. Physiol Res. 2009; 58(Suppl 2):S119–139. [PubMed: 20131930]

Dai J, Losy F, Guinault AM, Pages C, Anegon I, Desgranges P, Becquemin JP, Allaire E. Overexpression of transforming growth factor-beta1 stabilizes already-formed aortic aneurysms: a first approach to induction of functional healing by endovascular gene therapy. Circulation. 2005; 112:1008–1015. [PubMed: 16103255]

Davidson JM, LuValle PA, Zoia O, Quaglino D Jr, Giro M. Ascorbate differentially regulates elastin and collagen biosynthesis in vascular smooth muscle cells and skin fibroblasts by pretranslational mechanisms. J Biol Chem. 1997; 272:345–352. [PubMed: 8995268]

denBraber ET, deRuijter JE, Smits HTJ, Ginsel LA, vonRecum AF, Jansen JA. Quantitative analysis of cell proliferation and orientation on substrata with uniform parallel surface micro-grooves. Biomaterials. 1996; 17:1093–1099. [PubMed: 8718969]

Dobrin PB. Mechanical-Properties of Arteries. Physiol Rev. 1978; 58:397–460. [PubMed: 347471]

Dong Y, Yong T, Liao S, Chan CK, Stevens MM, Ramakrishna S. Distinctive degradation behaviors of electrospun polyglycolide, poly(DL-lactide-co-glycolide), and poly(L-lactide-co-epsilon-caprolactone) nanofibers cultured with/without porcine smooth muscle cells. Tissue Eng Part A. 2010; 16:283–298. [PubMed: 19839726]

Faury G, Garnier S, Weiss AS, Wallach J, Fulop T Jr, Jacob MP, Mecham RP, Robert L, Verdetti J. Action of tropoelastin and synthetic elastin sequences on vascular tone and on free Ca2+ level in human vascular endothelial cells. Circ Res. 1998; 82:328–336. [PubMed: 9486661]

Fornieri C, Baccarani-Contri M, Quaglino D Jr, Pasquali-Ronchetti I. Lysyl oxidase activity and elastin/glycosaminoglycan interactions in growing chick and rat aortas. J Cell Biol. 1987; 105:1463–1469. [PubMed: 2888772]

Fornieri C, Quaglino D Jr, Mori G. Role of the extracellular matrix in age-related modifications of the rat aorta. Ultrastructural, morphometric, and enzymatic evaluations. Arterioscler Thromb. 1992; 12:1008–1016. [PubMed: 1356019]

Gacchina CE, Ramamurthi A. Impact of pre-existing elastic matrix on TGFbeta1 and HA oligomer-induced regenerative elastin repair by rat aortic smooth muscle cells. J Tissue Eng Regen Med. 2011; 5:85–96. [PubMed: 20653044]

Gao J, Crapo P, Nerem R, Wang Y. Co-expression of elastin and collagen leads to highly compliant engineered blood vessels. J Biomed Mater Res A. 2008; 85:1120–1128. [PubMed: 18412137]

Hoenig MR, Campbell GR, Rolfe BE, Campbell JH. Tissue-engineered blood vessels: alternative to autologous grafts? Arterioscler Thromb Vasc Biol. 2005; 25:1128–1134. [PubMed: 15705929]

Holzapfel GA, Sommer G, Gasser CT, Regitnig P. Determination of layer-specific mechanical properties of human coronary arteries with nonatherosclerotic intimal thickening and related constitutive modeling. Am J Physiol Heart Circ Physiol. 2005; 289:H2048–2058. [PubMed: 16006541]

Hu JJ, Ambrus A, Fossum TW, Miller MW, Humphrey JD, Wilson E. Time courses of growth and remodeling of porcine aortic media during hypertension: a quantitative immunohistochemical examination. J Histochem Cytochem. 2008; 56:359–370. [PubMed: 18071063]

Isogai Z, Aspberg A, Keene DR, Ono RN, Reinhardt DP, Sakai LY. Versican interacts with fibrillin-1 and links extracellular microfibrils to other connective tissue networks. J Biol Chem. 2002; 277:4565–4572. [PubMed: 11726670]

Joddar B, Ramamurthi A. Elastogenic effects of exogenous hyaluronan oligosaccharides on vascular smooth muscle cells. Biomaterials. 2006; 27:5698–5707. [PubMed: 16899292]

Joddar B, Ramamurthi A. Fragment size- and dose-specific effects of hyaluronan on matrix synthesis by vascular smooth muscle cells. Biomaterials. 2006; 27:2994–3004. [PubMed: 16457881]

Johnson DJ, Robson P, Hew Y, Keeley FW. Decreased elastin synthesis in normal development and in long-term aortic organ and cell cultures is related to rapid and selective destabilization of mRNA for elastin. Circ Res. 1995; 77:1107–1113. [PubMed: 7586222]

Kothapalli CR, Ramamurthi A. Lysyl oxidase enhances elastin synthesis and matrix formation by vascular smooth muscle cells. J Tissue Eng Regen Med. 2009; 3:655–661. [PubMed: 19813219]

Kothapalli CR, Taylor PM, Smolenski RT, Yacoub MH, Ramamurthi A. Transforming growth factor beta 1 and hyaluronan oligomers synergistically enhance elastin matrix regeneration by vascular smooth muscle cells. Tissue Eng Part A. 2009; 15:501–511. [PubMed: 18847364]

Labarca C, Paigen K. A simple, rapid, and sensitive DNA assay procedure. Anal Biochem. 1980; 102:344–352. [PubMed: 6158890]

Lee JY, Bashur CA, Goldstein AS, Schmidt CE. Polypyrrole-coated electrospun PLGA nanofibers for neural tissue applications. Biomaterials. 2009; 30:4325–4335. [PubMed: 19501901]

Lee JY, Bashur CA, Gomez N, Goldstein AS, Schmidt CE. Enhanced polarization of embryonic hippocampal neurons on micron scale electrospun fibers. J Biomed Mater Res A. 2009

Li DY, Brooke B, Davis EC, Mecham RP, Sorensen LK, Boak BB, Eichwald E, Keating MT. Elastin is an essential determinant of arterial morphogenesis. Nature. 1998; 393:276–280. [PubMed: 9607766]

Li S, Lao J, Chen BP, Li YS, Zhao Y, Chu J, Chen KD, Tsou TC, Peck K, Chien S. Genomic analysis of smooth muscle cells in 3-dimensional collagen matrix. FASEB J. 2003; 17:97–99. [PubMed: 12475912]

Livak KJ, Schmittgen TD. Analysis of relative gene expression data using real-time quantitative PCR and the 2(-Delta Delta C(T)) Method. Methods. 2001; 25:402–408. [PubMed: 11846609]

Lloyd-Jones D, Adams R, Carnethon M, De Simone G, Ferguson TB, Flegal K, Ford E, Furie K, Go A, Greenlund K, Haase N, Hailpern S, Ho M, Howard V, Kissela B, Kittner S, Lackland D, Lisabeth L, Marelli A, McDermott M, Meigs J, Mozaffarian D, Nichol G, O'Donnell C, Roger V, Rosamond W, Sacco R, Sorlie P, Stafford R, Steinberger J, Thom T, Wasserthiel-Smoller S, Wong N, Wylie-Rosett J, Hong Y. Heart disease and stroke statistics--2009 update: a report from the American Heart Association Statistics Committee and Stroke Statistics Subcommittee. Circulation. 2009; 119:e21–181. [PubMed: 19075105]

Losy F, Dai J, Pages C, Ginat M, Muscatelli-Groux B, Guinault AM, Rousselle E, Smedile G, Loisance D, Becquemin JP, Allaire E. Paracrine secretion of transforming growth factor-beta1 in aneurysm healing and stabilization with endovascular smooth muscle cell therapy. J Vasc Surg. 2003; 37:1301–1309. [PubMed: 12764279]

Majack RA, Goodman LV, Dixit VM. Cell surface thrombospondin is functionally essential for vascular smooth muscle cell proliferation. J Cell Biol. 1988; 106:415–422. [PubMed: 2448314]

Majack RA, Majesky MW, Goodman LV. Role of PDGF-A expression in the control of vascular smooth muscle cell growth by transforming growth factor-beta. J Cell Biol. 1990; 111:239–247. [PubMed: 1694856]

Marshall OJ. PerlPrimer: cross-platform, graphical primer design for standard, bisulphite and real-time PCR. Bioinformatics. 2004; 20:2471–2472. [PubMed: 15073005]

McMahon MP, Faris B, Wolfe BL, Brown KE, Pratt CA, Toselli P, Franzblau C. Aging effects on the elastin composition in the extracellular matrix of cultured rat aortic smooth muscle cells. In Vitro Cell Dev Biol. 1985; 21:674–680. [PubMed: 3908442]

Nair LS, Laurencin CT. Biodegradable polymers as biomaterials. Progress in Polymer Science. 2007; 32:762–798.

Olin AI, Morgelin M, Sasaki T, Timpl R, Heinegard D, Aspberg A. The proteoglycans aggrecan and Versican form networks with fibulin-2 through their lectin domain binding. J Biol Chem. 2001; 276:1253–1261. [PubMed: 11038354]

Pardali E, Goumans MJ, ten Dijke P. Signaling by members of the TGF-beta family in vascular morphogenesis and disease. Trends Cell Biol. 2010; 20:556–567. [PubMed: 20656490]

Patel A, Fine B, Sandig M, Mequanint K. Elastin biosynthesis: The missing link in tissue-engineered blood vessels. Cardiovasc Res. 2006; 71:40–49. [PubMed: 16566911]

Pektok E, Nottelet B, Tille JC, Gurny R, Kalangos A, Moeller M, Walpoth BH. Degradation and healing characteristics of small-diameter poly(epsilon-caprolactone) vascular grafts in the rat systemic arterial circulation. Circulation. 2008; 118:2563–2570. [PubMed: 19029464]

Peyton SR, Kim PD, Ghajar CM, Seliktar D, Putnam AJ. The effects of matrix stiffness and RhoA on the phenotypic plasticity of smooth muscle cells in a 3-D biosynthetic hydrogel system. Biomaterials. 2008; 29:2597–2607. [PubMed: 18342366]

Richard MN, Deniset JF, Kneesh AL, Blackwood D, Pierce GN. Mechanical stretching stimulates smooth muscle cell growth, nuclear protein import, and nuclear pore expression through mitogen-activated protein kinase activation. J Biol Chem. 2007; 282:23081–23088. [PubMed: 17525165]

Sajid M, Lele M, Stouffer GA. Autocrine thrombospondin partially mediates TGF-beta1- induced proliferation of vascular smooth muscle cells. Am Physiol Heart Circ Physiol. 2000; 279:H2159–2165.

Stankus JJ, Guan J, Fujimoto K, Wagner WR. Microintegrating smooth muscle cells into a biodegradable, elastomeric fiber matrix. Biomaterials. 2006; 27:735–744. [PubMed: 16095685]

Stegemann H, Stalder K. Determination of hydroxyproline. Clin Chim Acta. 1967; 18:267–273. [PubMed: 4864804]

Stegemann JP, Nerem RM. Altered response of vascular smooth muscle cells to exogenous biochemical stimulation in two- and three-dimensional culture. Exp Cell Res. 2003; 283:146–155. [PubMed: 12581735]

Tan EPS, Ng SY, Lim CT. Tensile testing of a single ultrafine polymeric fiber. Biomaterials. 2005; 26:1453–1456. [PubMed: 15522746]

Vaz CM, van Tuijl S, Bouten CV, Baaijens FP. Design of scaffolds for blood vessel tissue engineering using a multi-layering electrospinning technique. Acta Biomater. 2005; 1:575–582. [PubMed: 16701837]

Wang JHC, Jia FY, Gilbert TW, Woo SLY. Cell orientation determines the alignment of cell-produced collagenous matrix. Journal of Biomechanics. 2003; 36:97–102. [PubMed: 12485643]

Worth NF, Rolfe BE, Song J, Campbell GR. Vascular smooth muscle cell phenotypic modulation in culture is associated with reorganisation of contractile and cytoskeletal proteins. Cell Motil Cytoskeleton. 2001; 49:130–145. [PubMed: 11668582]

Yang F, Murugan R, Wang S, Ramakrishna S. Electrospinning of nano/micro scale poly(L-lactic acid) aligned fibers and their potential in neural tissue engineering. Biomaterials. 2005; 26:2603–2610. [PubMed: 15585263]

Yeung T, Georges PC, Flanagan LA, Marg B, Ortiz M, Funaki M, Zahir N, Ming W, Weaver V, Janmey PA. Effects of substrate stiffness on cell morphology, cytoskeletal structure, and adhesion. Cell Motil Cytoskeleton. 2005; 60:24–34. [PubMed: 15573414]

Zhang X, Baughman CB, Kaplan DL. In vitro evaluation of electrospun silk fibroin scaffolds for vascular cell growth. Biomaterials. 2008; 29:2217–2227. [PubMed: 18279952]

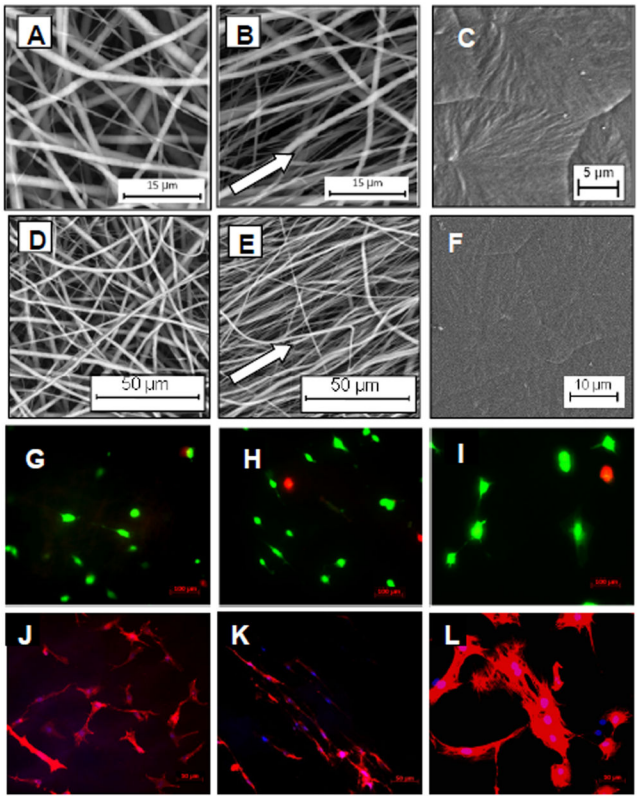

Figure 1.

PCL substrate structure and RASMC morphology. Shown are SEM images of meshes electrospun from 18% w/v PCL solution on a drum rotating at 30 (A, D) and 1600 rpm (B, E) to produce random and aligned meshes, respectively. Smooth spin-coated surfaces (controls) are shown in (C, F). Live/Dead (green/red) staining of RASMCs after 6 days of culture on random meshes (G), aligned meshes (H), and spin-coated controls (I) showed significant cell viability and immunofluorescent images of cell nuclei/SM22α (blue/red) on random (J), aligned (K), and spin-coated surfaces (L) showed cell morphology and alignment.

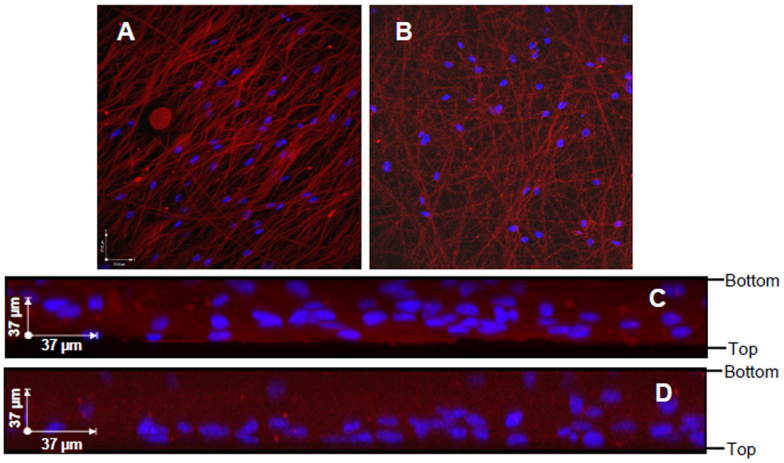

Figure 2.

Cell infiltration within aligned (A, C) and random (B, D) electrospun PCL meshes. DAPI labeled nuclei appear blue and DiI stained meshes appear red. Shown are 3-D x–y plane projections of a series of confocal images acquired at 1 μm intervals throughout the thickness of the scaffolds (A–B) and maximum projections on the x–z plane (C–D). The edges of the meshes and the seeding orientation are marked on the right-hand side.

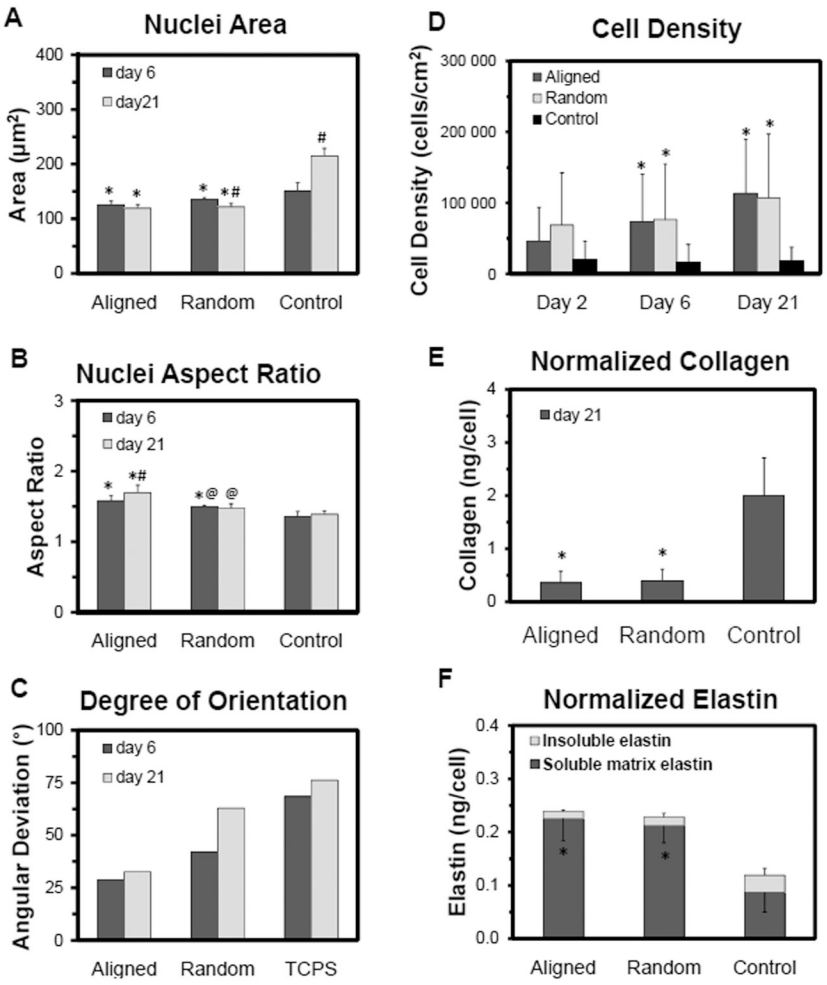

Figure 3.

Impact of substrate topography on RASMC morphology at 6 and 21 days of culture and on RASMC proliferation and matrix production at 21 days of culture. Nuclear area (A), aspect ratio (B), and degree of orientation (C) were quantified from DAPI-labeled nuclei. Biochemical analysis of RASMCs density as determined from DNA content (D), collagen content determined with a hydroxyl-proline assay (E), and soluble (bottom error bar) and insoluble matrix (top error bar – standard error) elastin content/cell as determined with the Fastin® assay (F). The study was replicated, n = 6 samples/condition/replicate and n = 12 samples/condition total. * indicates statistical difference from the spin-coated films, # indicates statistical difference from day 6, and @ indicates statistical difference from the aligned mesh.

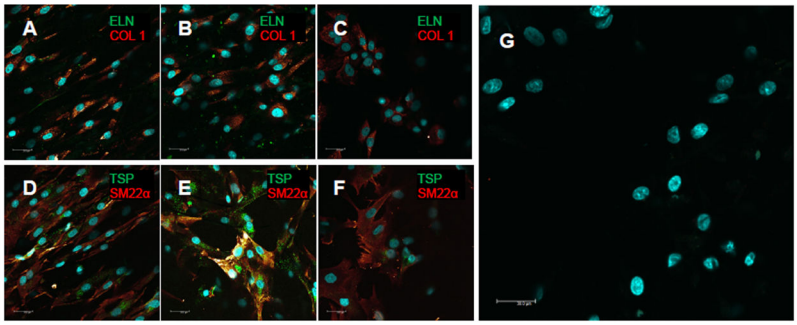

Figure 4.

Impact of substrate topography on RASMC phenotype and matrix production. Representative confocal images of RASMCs after 21 days on aligned meshes (A, D), random meshes (B, E, G), and spin-coated controls (C, F). The cells stained (green/red) for markers of both contractile (i.e. SM22α) and activated (i.e. thrombospondin (TSP)) SMC phenotypes. Cells cultured on meshes and controls also stained for collagen type 1 (COL 1, localized in the cell) and trace amounts of elastin (ELN). Image (G) is a representative negative immunofluorescent control that did not receive any primary antibodies. Cell nuclei were labeled with DAPI (blue).

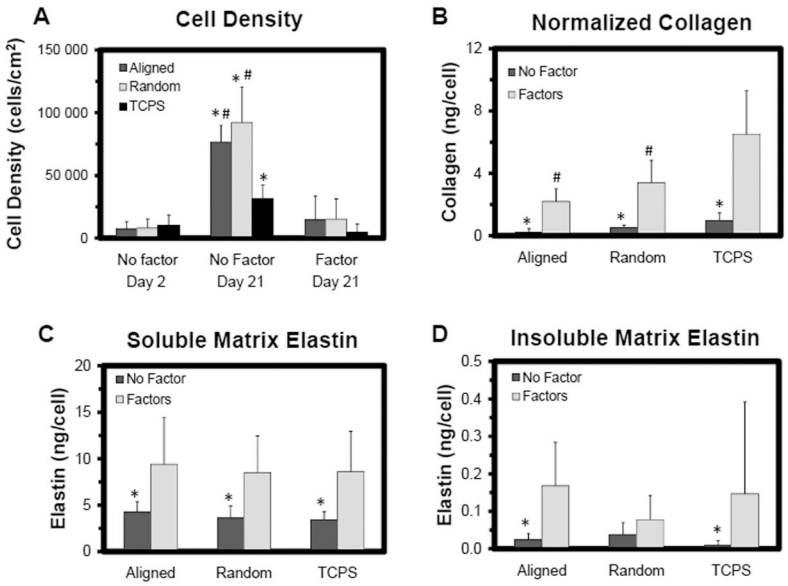

Figure 5.

Biochemical analysis of RASMCs cultured on samples with and without elastogenic factors. Shown are RASMCs density as determined from DNA content (A), collagen content determined with a hydroxyl-proline assay (B), and alkali-soluble (C) and alkali-insoluble matrix (D) elastin synthesis per cell as determined with the Fastin®; assay. Cells were cultured for 21 days (the study was replicated, n = 3 samples/condition/replicate and n = 6 samples/condition total). * indicates statistical difference from the samples with exogenous factors added, and # indicates statistical difference from the TCPS condition.

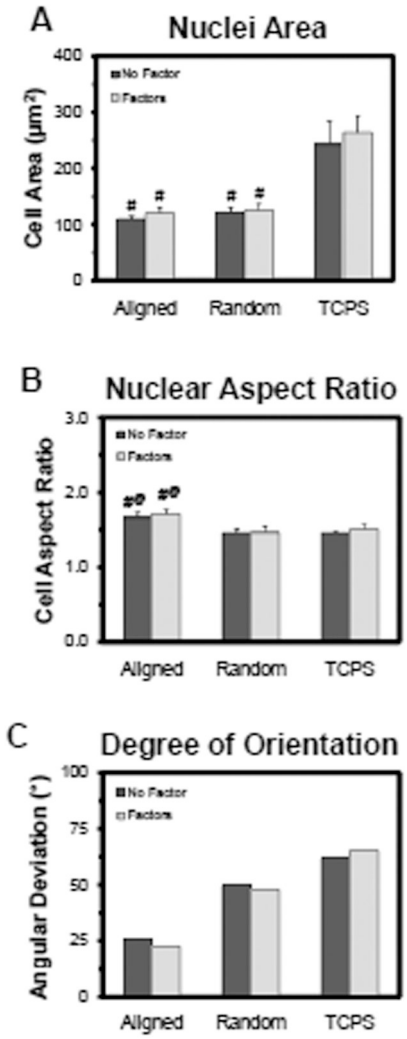

Figure 6.

Impact of exogenous factors on RASMC morphology after 21 days of culture. Nuclear cell area (A), aspect ratio (B), and degree of orientation (C) as quantified from DAPI-labeled nuclei. * indicates statistical difference from the samples with exogenous factors added, # indicates statistical difference from the TCPS condition, and @ indicates statistical difference from the aligned mesh.

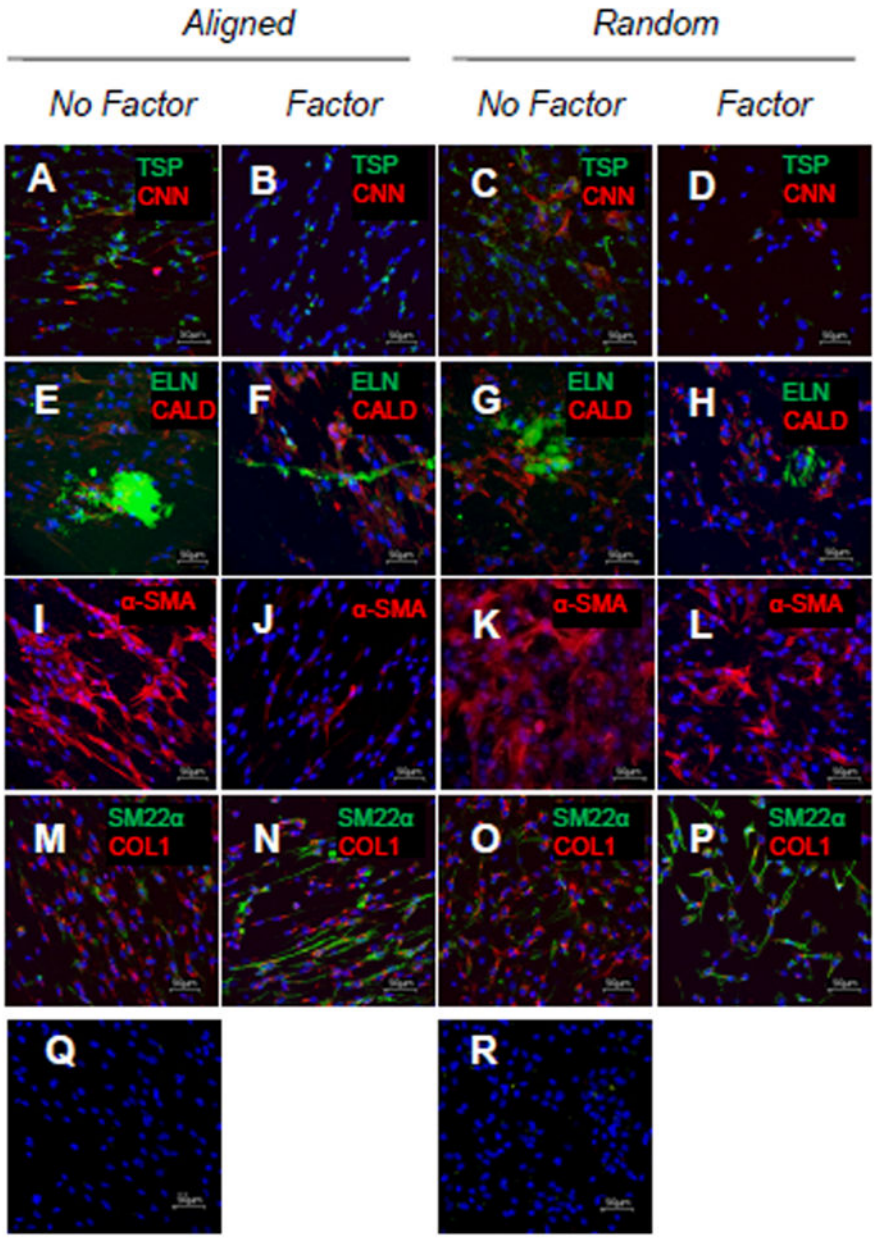

Figure 7.

Impact of exogenous factors on RASMC phenotype and matrix production after 21 days of culture. Representative confocal projections of RASMCs cultured on aligned meshes without (A, E, I, M, and Q) and with (B, F, J, and N) factors, and random meshes without (C, G, K, and O) and with (D, H, L, P, and R) factors. The markers (green/red) are thrombospondin (TSP)/calponin (CNN) (A–D), elastin (ELN)/caldesmon (E–H), nothing/α-SMA (α-SMA) (I–L), and SM22α/collagen type 1 (COL 1) (M–P). Images (Q–R) are negative immunofluorescent controls that did not receive any primary antibodies. Cell nuclei were labeled with DAPI (blue). The images are max projections of confocal slices acquired at 1μm intervals across the thickness of the meshes.

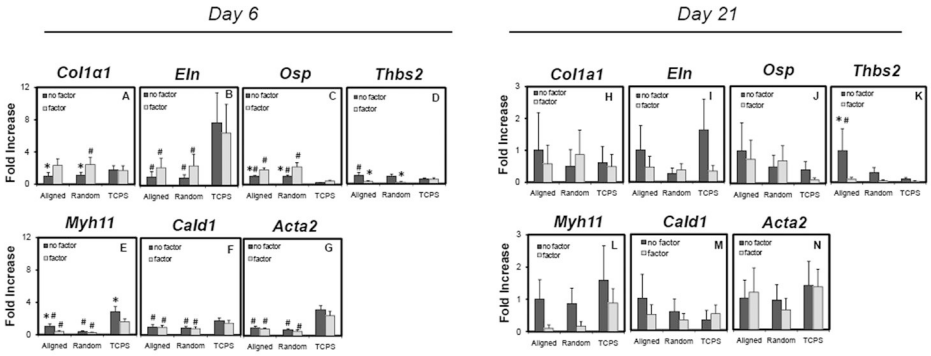

Figure 8.

RT-PCR outcomes showing fold differences in mRNA expression of matrix components and phenotypic markers by RASMCs at an early culture time (i.e. day 6) (A–G) and at a later culture time (i.e. day 21) (H–N). The specific genes are *Col1a1* (A and H), *Eln* (B and I), *Osp* (C and J), *Thbs2* (D and K), *Myh11* (E and L), *Cald1* (F and M), and *Acta2* (G and N). The values are reported as $2^{-\Delta\Delta Ct}$, and the bars are standard error of the mean. * indicates statistical difference relative to cells cFultured with exogenous factors, and # indicates statistical difference relative to culture on TCPS.

Table 1

Primer sequences designed for real time-PCR

Gene	Forward Primer (5′ --> 3′)	Forward Primer (3′ --> 5′)	Product Size (bp)
Osp	TAAGCAAGAAACTCTTCCAAGC	AGGACTCATCAGATTCATCGG	157
Thbs2	CAGATCAGATGGATCAGGAC	GTTGGAGTTGGAGATGTATGG	118
Cald1	GAGAGGAGGAAGAGAAGAGGA	CACTTGAACGGCTTCTTGTC	120
Myh11	TGCTACAAGATCGTGAAGAC	CTTTCTTGCCTTTGTGGGAG	125
Acta2	ATAGAACACGGCATCATCAC	GTCTCAAACATAATCTGGGTC	166